Sliding drops in the diffuse interface model coupled to hydrodynamics

Uwe Thiele and Manuel G. Velarde
Instituto Pluridisciplinar, Universidad Complutense, Paseo Juan XXIII, 1, 28040 Madrid, Spain

Kai Neuffer
Instituto Pluridisciplinar, Universidad Complutense, Paseo Juan XXIII, 1, 28040 Madrid, Spain
and Lehrstuhl für Statistische Physik und Nichtlineare Dynamik, BTU-Cottbus, Erich-Weinert-Strasse 1, 03046 Cottbus, Germany

Michael Bestehorn
Lehrstuhl für Statistische Physik und Nichtlineare Dynamik, BTU-Cottbus, Erich-Weinert-Strasse 1, 03046 Cottbus, Germany

Yves Pomeau
Instituto Pluridisciplinar, Universidad Complutense, Paseo Juan XXIII, 1, 28040 Madrid, Spain
and Laboratoire de Physique Statistique de l'Ecole Normale Supérieure, associè au CNRS, 24 Rue Lhomond, 75231 Paris Cedex 05, France

(Received 8 June 2001; revised manuscript received 28 August 2001; published 20 November 2001)

Using a film thickness evolution equation derived recently combining long-wave approximation and diffuse interface theory [L. M. Pismen and Y. Pomeau, Phys. Rev. E **62**, 2480 (2000)] we study one-dimensional surface profiles for a thin film on an inclined plane. We discuss stationary flat film and periodic solutions including their linear stability. Flat sliding drops are identified as universal profiles, whose main properties do not depend on mean film thickness. The flat drops are analyzed in detail, especially how their velocity, advancing and receeding dynamic contact angles and plateau thicknesses depend on the inclination of the plane. A study of nonuniversal drops shows the existence of a dynamical wetting transition with hysteresis between droplike solutions and a flat film with small amplitude nonlinear waves.

DOI: 10.1103/PhysRevE.64.061601 PACS number(s): 68.15.+e, 68.55.−a, 47.55.Dz, 64.70.−p

I. INTRODUCTION

Much interest has focused recently on structure formation in thin liquid films. Two especially well-investigated problems are the rupture and dewetting of very thin liquid films and the formation of waves and localized structures in a film flowing down an inclined plane [1].

If a liquid is deposited on a surface where this situation is energetically unfavorable (non- or partially wetting), after some transient, the liquid is collected in drops on the surface. The resulting contact angle formed by the solid-liquid and the liquid-gas interface is determined by the various molecular interactions. For relatively large drops it is given by a combination of the various surface tensions (Young-Laplace relation) [2]. However, for very small thicknesses (<100 nm) distance-dependent molecular interactions have to be introduced explicitly in the hydrodynamic formalism. This is achieved by an additional pressure term, the disjoining pressure [3,4]. Depending on the particular problem treated, this disjoining pressure may incorporate long-range van-der-Waals and/or various types of short-range interaction terms [5–8].

If the deposited liquid forms a thin film on the substrate, the transition towards drops is initiated by film rupture caused by a surface instability (spinodal dewetting [9]) or by nucleation at defects. Lateral growth of the resulting holes yields a network of liquid rims that decays later into small drops [10]. The process and the resulting structures are in principle, well understood. The methods employed range from linear stability analysis [11] to fully nonlinear analysis by one- and two-dimensional numerical simulations of the time evolution of the film thickness profile [12–14]. If the liquid is already deposited in drop form it may relax towards equilibrium by spreading or retracting [1,2,15,16]. Both the spreading of a drop and the growth of a hole involve the movement of a three-phase contact line. The classical no-slip boundary condition at the liquid-solid interface makes the movement of the contact line impossible if the contact line is considered as a material line. This problem may be circumvented by introducing a very thin precursor film or allowing for a slip near the contact line [2,17].

Experiments on liquid films that flow down an inclined plane (falling films) studied the formation of waves [18], localized structures, and their interaction [19]. Linear stability analysis [20,21], weakly nonlinear analysis [22–24], the study of sideband instabilities [25], and solitary waves [26] already revealed many important features. However, the studies focus on structure formation caused by inertia measured by the Reynolds number. Thereby the molecular interactions between film and substrate are neglected so that this type of description cannot apply to very thin films.

This is also the case for most works that focus on the evolution of falling sheets or ridges [27,28], i.e., the advancing edge of a fluid film or long one-dimensional drops on an inclined ''dry'' substrate. As for the spreading drop, a precursor film or slip at the substrate [29–31] helps to avoid divergence problems at the contact line, but introduces new ad hoc parameters into the model. The additional parameters, namely, the slip length or the precursor film thickness have an influence on the base state profiles and on the transverse

front instability (growth rate and fastest growing wave number) [31–34]. Also, the equilibrium and dynamic contact angles remain to be fixed independently in this kind of theory [30,35,36]. In an alternative approach [37], either the vapor-liquid or fluid-solid interface, or both, are treated as a separate phase with properties that differ from the bulk fluid. A droplet of nonwetting viscous liquid rolling along an inclined plane was studied in [38,39]. They showed that the classical stress singularity at the contact line is alleviated in this case. Recent experiments on drops sliding down an inclined plane showed the existence of stationary drops that slide down the plane without changing their shape [40].

Recently, Pismen and Pomeau combined the long-wave approximation for thin films [1] with a diffuse interface description for the liquid-gas interface [41] and derived a film thickness equation incorporating a disjoining pressure term without divergence for vanishing film thickness [42]. First, they discuss the vertical density profile for the liquid in a flat horizontal layer of fluid incorporating the smooth but nevertheless relatively sharp density transition between fluid and gas, and the density variation close to the solid substrate due to molecular interactions that enter into the calculation via the boundary condition for the fluid density at the substrate [43]. Then they combine in a fully consistent theory the obtained density profile with the Stokes equation in the long-wave approximation to account for dynamical situations. The resulting film thickness equation has the usual form of a thin-film equation with disjoining pressure [1], where the disjoining pressure now results from diffuse interface theory in a purely hydrodynamic derivation. It is not introduced ad hoc into the hydrodynamic formalism and does not suffer from a divergence for vanishing film thickness as all the other disjoining pressures known to the authors. The theory is fully consistent with Stokes equation of fluid mechanics and with Young-Laplace equilibrium theory in its van der Waals formulation.

The evolution equation was used to study the structure formation in an unstable liquid film on a horizontal solid substrate [44]. Below, the same equation is used to study structure formation in a flowing film on a slightly inclined plane. In contrast to the above-mentioned contributions on falling films inertia is irrelevant here and the structures result from molecular interaction between film and substrate and the viscous flow due to the inclination of the plane. One advantage of this approach is the close resemblance of the governing equations for the horizontal and the inclined case, which gives a good starting point for the interpretation of different types of stationary solutions. Furthermore, the study gives an example of the effect of breaking the reflection symmetry on structure formation.

In Sec. II, we discuss the evolution equation for the film thickness and introduce the scaling. Then, we derive a stationary equation, discuss flat film solutions and their stability (Sec. III) and calculate the families of stationary periodic solutions of finite amplitude (Sec. IV). We identify solitary wavelike solutions and nucleation solutions by means of linear stability analysis and nonlinear analysis. Within the different solution families solutions with universal behavior are identified. We call these solutions, that resemble *flat sliding drops*, "universal" because their main properties (velocity, amplitude, and dynamic contact angles) do not depend on the choosen mean film thickness. The dependence of their properties on the inclination angle is investigated in detail (Sec. IV B). The limits of the flat-drop regime and the nonuniversal solutions, whose properties depend also on mean film thickness, that prevail outside of this regime are discussed in Sec. IV C. In the conclusion (Sec. V), the relation with experiments and related theoretical work is discussed.

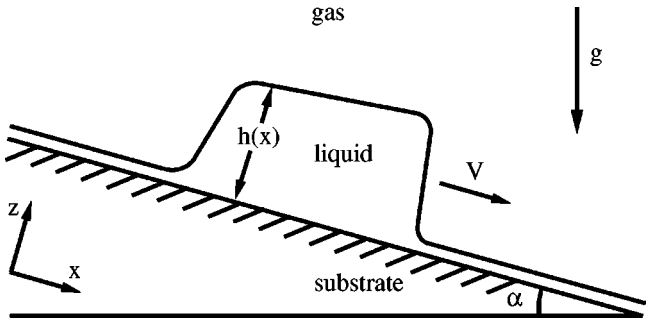

FIG. 1. Sketch of the geometry.

II. FILM THICKNESS EQUATION

We use the film evolution equation as derived by PISMEN and POMEAU [42] to study the structure formation in a thin liquid film flowing down an inclined plane. For a two-dimensional geometry as sketched in Fig. 1, the equation writes

$$\partial_t h = -\partial_x (Q(h)\{\partial_x[\gamma \partial_{xx} h - \partial_h f(h,a)] + \bar{\alpha}\rho g\}), \quad (1)$$

where $h(x,t)$ denotes the x-dependent film thickness, g is the gravitational acceleration, $Q(h)=h^3/3\eta$ is the mobility factor due to Poiseuille flow, $\bar{\alpha}$ is the small inclination angle between the plane and the horizontal, and ρ, γ, and η are the respective density, surface tension, and viscosity of the liquid. x is the coordinate along the inclined plane increasing downwards. Subscripts t, x, and h denote the corresponding partial derivatives. Furthermore,

$$\partial_h f(h,a) = \kappa M(h,a) + \rho g h = \frac{2\kappa}{a} e^{-h/l}\left(1 - \frac{1}{a} e^{-h/l}\right) + \rho g h \quad (2)$$

is the derivative of the free energy $f(h,a)$ and has the dimension of pressure. $\Pi(h) = -\kappa M(h,a)$ is the disjoining pressure derived from diffuse interface theory [42], a is a small positive parameter describing the wetting properties in the regime of partial wetting, l is the length scale of the diffuse interface, and κ is the strength of the molecular interaction. The disjoining pressure resembles qualitatively the disjoining pressures that combine destabilizing short-range and stabilizing long-range interactions, without sharing their shortcomings as explained above in the Introduction.

Equation (1) has the form of a mass conservation law $\partial_t h = -\partial_x \Gamma(x,t)$, where $\Gamma(x,t)$ is the flow composed of (1) the flow due to the gradient of the Laplace or curvature pres-

sure $\gamma\partial_{xx}h$, (2) the flow due to gradients of additional pressure terms (resulting from molecular interactions $\kappa M(h,a)$ and hydrostatic pressure $\rho g h$), $\partial_h f(h,a)$, and (3) the gravitationally driven flow down the inclined plane, $\overline{\alpha}\rho g$.

To use dimensionless quantities (with tilde), suitable scales are used

$$t=\frac{3\eta\gamma}{\kappa^2 l}\tilde{t},$$

$$h=l\tilde{h}, \tag{3}$$

$$x=\sqrt{\frac{l\gamma}{\kappa}}\tilde{x}.$$

The ratio $\kappa l/\gamma$ is $O(a^2)$ [42], i.e., the scale in the x direction is l/a. We find after dropping the tildes

$$\partial_t h=-\partial_x\{h^3(\partial_x[\partial_{xx}h-M(h,a)-Gh]+\alpha G)\}, \tag{4}$$

where

$$G=\frac{l\rho g}{\kappa} \quad \text{and} \quad \alpha=\overline{\alpha}\left(\frac{\gamma}{\kappa l}\right)^{1/2}. \tag{5}$$

G gives the ratio between gravitation and molecular interactions. Here, its value is always taken positive. Note, that α is no longer a small parameter. The form of $M(h,a)$ allows us to transfer the constant a into the mobility factor Q by the transformation $\overline{h}=h+\ln a$. Using this shift enables us to directly compare the given results with the study of the thin liquid film on a horizontal, noninclined substrate [44].

After dropping the bar, the evolution Eq. (1) becomes

$$\partial_t h=-\partial_x\{(h-\ln a)^3(\partial_x[\partial_{xx}h-\partial_h f(h)]+\alpha G)\} \tag{6}$$

with

$$\partial_h f(h)=2e^{-h}(1-e^{-h})+Gh. \tag{7}$$

In the following, we use only dimensionless quantities if not otherwise stated.

III. STATIONARY SOLUTIONS

To study stationary solutions for the film thickness profile $h(x,t)$ that move with the dimensionless velocity v we use the comoving coordinate system $x_{co}=x-vt$, implying $\partial_t h=-v\partial_x h$. Integration of Eq. (6) in the comoving frame yields

$$0=Q(h,a)(\partial_{xxx}h-\partial_{hh}f\partial_x h)+\alpha GQ(h,a)-vh+C_0. \tag{8}$$

The mobility factor is now $Q(h,a)=(h-\ln a)^3$ and C_0 is a constant of integration. In contrast to the reflection symmetric problem of film rupture on a horizontal plane [44], here we cannot set $C_0=0$ and consequentely cannot integrate another time. Writing Eq. (8) in the form $(\Gamma-vh)+C_0=0$ tells us that for all stationary solutions, the flow in the comoving frame $\Gamma-vh$ is constant with respect to x but not the flow in the laboratory system Γ. The choice of the constant of integration,

$$C_0=-(\Gamma_0-vh_0)=-Q(h_0,a)\alpha G+vh_0, \tag{9}$$

introduces a flat film or homogeneous solution of thickness h_0 and the corresponding flow in the laboratory system $\Gamma_0=-Q(h_0,a)\alpha G$ in a natural way. This corresponds to prescribing the liquid volume.

A. Flat film solutions

Beside the flat-film solution given by the choice of h_0, there may exist other film thicknesses h_i with corresponding flow in the laboratory system Γ_i that give the same flow in the comoving frame, $C_0=\Gamma_i-vh_i=\Gamma_0-vh_0$. Take note, that flat film solutions correspond to the fixed points of Eq. (8), seen as a dynamical system. Given the flow Γ_0 by prescribing h_0 there exist two more fixed points of this dynamical system

$$h_{1,2}=(h_0-\ln a)\left(-\frac{1}{2}\pm\sqrt{\frac{v}{G\alpha(h_0-\ln a)^2}-\frac{3}{4}}\right)+\ln a. \tag{10}$$

Because the physical film thickness $h-\ln a$ has to be positive everywhere, one has to choose the positive sign in Eq. (10). This solution gives a positive fixed point for $v/G\alpha(h_0-\ln a)^2>1$, i.e., a second flat-film solution corresponding to the conjugate solution in, for instance, [45]. For $v/G\alpha(h_0-\ln a)^2>3$, its thickness is larger than the given film thickness $h_0-\ln a$. Note that the location of the fixed points does not depend on the molecular interaction $M(h)$. However, it does depend on it for the limiting case $\alpha=0$ [44]. The consequences will be discussed below in Sec. IV B.

B. Linear stability of flat-film solutions

The linear stability of the flat-film solutions to harmonic perturbations is determined by using the ansatz $h(x)=h_0+\epsilon\exp(\beta t+ikx)$ to linearize the time-dependent Eq. (6). This yields for the dispersion relation $\beta(k)$

$$\beta=-(h_0-\ln a)^3k^2(k^2+f_{hh}|_{h_0})-i3\alpha Gk(h_0-\ln a)^2, \tag{11}$$

where $f_{hh}|_{h_0}$ is short for $\partial_{hh}f(h)|_{h=h_0}$. The real and imaginary parts of $\beta(k)$ give the respective growth rate and downwards phase velocity of the mode with wave-number k. The flat film is unstable for $\mathrm{Re}\,\beta>0$. Using Eq. (7) yields linear instability for

$$f_{hh}(h_0)=-2e^{-h_0}(1-2e^{-h_0})+G<0, \tag{12}$$

i.e., for an intermediate thickness range

$$h_-<h_0<h_+, \tag{13}$$

where

$$h_{\pm} = -\ln\left[\frac{1}{2}\left(\frac{1}{2} \mp \sqrt{\frac{1}{4} - G}\right)\right]. \tag{14}$$

In contrast to the existence of flat-film solutions, their stability does not depend on the dynamical aspect of the problem (tilt angle and velocity), but only on $f_{hh}(h)$ as for a flat film on a horizontal substrate [44]. In the limit of vanishing influence of the disjoining pressure, this corresponds to the fact that we only regard Stokes flow (the Reynolds number is zero in our scaling), i.e., without the disjoining pressure the flat film would be linearly stable for all inclination angles. The critical wave-number, k_c given by $\beta=0$ is $k_c = \sqrt{-f_{hh}(h_0)}$, whereas the fastest growing mode has the wave-number $k_m = k_c/\sqrt{2}$ with growth rate $\beta_m = (h_0 - \ln a)^3 f_{hh}(h_0)^2/4$. For $G \ll 1$, one finds $h_- \approx -\ln(G/2)$ and $h_+ \approx \ln 2 + G$. There is a critical point at $(G_c = 1/4, h_c = \ln 4)$ where the lower- and the upper-linear instability lines meet. For $G > G_c$, flat films are always linearly stable.

All linear modes propagate downwards with the velocity $v = -\operatorname{Im}\beta/k = 3\alpha G(h_0 - \ln a)^2$, corresponding to the fluid velocity at the surface of the unperturbed flat film.

IV. PERIODIC AND LOCALIZED SOLUTIONS

Given a flat film in the linearly unstable thickness range, it will start to evolve in time. This may lead to film rupture or to a stationary film profile of finite amplitude, i.e., to nonlinear waves. These waves are stationary solutions of Eq. (6), i.e., solutions of Eq. (8). Periodic waves are found numerically using continuation methods [46] starting from small amplitude analytic solutions. The linear stability analysis of the periodic solutions will lead us to first conclusions about the physical meaning of the various occuring types. Direct integration Eq. (6) in time supports the given physical interpretation. Details of the numerical methods may be found in Appendix A.

A. Short-period solutions

Small amplitude stationary solutions take the form $h(x) = h_0 + \epsilon e^{ikx}$, as seen by linearizing Eq. (8). The resulting condition $0 = k^3 + f_{hh}(h_0)k - i[3\alpha G k(h_0 - \ln a)^2 - v k]$ implies $k = k_c = \sqrt{-f_{hh}(h_0)}$ and $v = 3\alpha G(h_0 - \ln a)^2$, corresponding to the neutrally stable modes obtained in the linear stability analysis in Sec. III B. Small-amplitude solutions exist only in the linearly unstable film thickness range.

We begin with a study of the stationary solutions at a fixed inclination angle α and given interaction parameters G and a. We keep, if not otherwise stated, $\alpha = 0.1$, $G = 0.1$, and $a = 0.1$. We are interested in the solution amplitude and velocity as a function of the period ($2\pi/k$ in the linear case) for different given mean film thicknesses $\bar{h}$. Depending on $\bar{h}$, qualitatively different families of solutions are found. Their velocity-period and amplitude-period dependencies are shown in Figs. 2 and 3, respectively. We call family the set of solutions for a given mean film thickness and classify them by the number and type of their branches, where branch stands for a part of a family that allows us to assign a unique value of velocity and amplitude to a given period. Branches

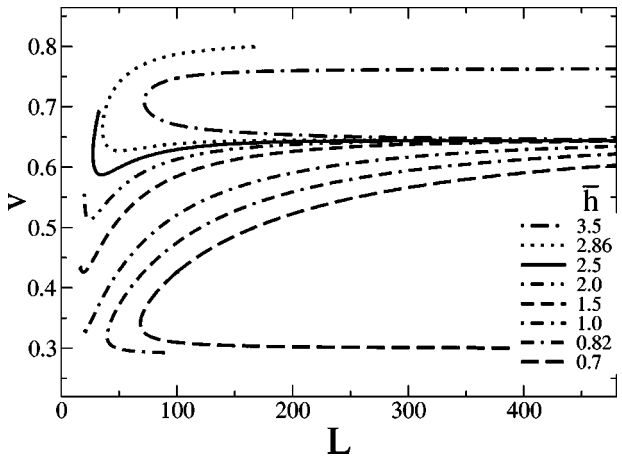

FIG. 2. Characterization of stationary periodic solutions. Shown is the dependence of the velocity v on period L for different mean film thicknesses, $\bar{h}$ as given in the legend. $G = 0.1$, $\alpha = 0.1$, and $a = 0.1$.

may show monotonic or nonmonotonic behavior of amplitude or/and velocity with respect to period.

In the following, the various family types are listed with increasing mean film thickness. The value given to $\bar{h}$ in the parenthesis refers, as an example, to Figs. 2 and 3.

(1) For very small $\bar{h}$, no solution exists beside the trivial $h(x) = h_0$.

(2) There are two branches with different velocities v and amplitudes A for the same period L. Both continue towards $L \to \infty$ and show a monotonic dependence of v and A on L $(\bar{h} = 0.7)$.

(3) There are two branches with different v and A, but only the branch with higher velocity continues towards $L \to \infty$. Both show a monotonic dependence of v on L. Considering the period as a bifurcation parameter, the endpoint of the branch with higher velocity and smaller amplitude corresponds to the locus of a subcritical bifurcation from uniform solutions to solutions oscillating in space $(\bar{h} = 0.82)$.

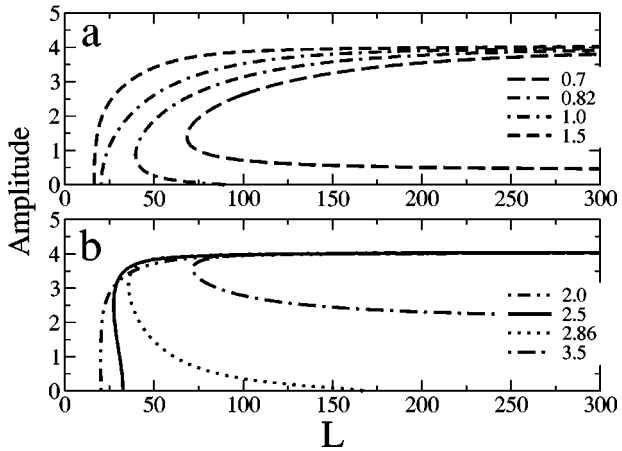

FIG. 3. Shown is the dependence of the amplitude on period L for the solution branches from Fig. 2. The legends of (a) and (b) give the respective mean film thicknesses.

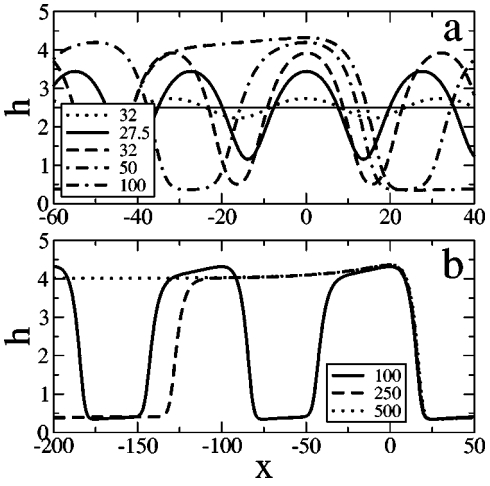

FIG. 4. Profiles for different periods L as shown in the legends of (a) and (b) at film thickness $\bar{h}=2.5$. $G=0.1$, $\alpha=0.1$, and $a=0.1$. Take note that in (a), the period changes non-monotonically with increasing amplitude. In (b), one can see the transition towards the flat drops.

(4) One branch exists that continues towards $L\rightarrow\infty$. Both v and A increase monotonously with L. The endpoint of the branch corresponds to the locus of a supercritical bifurcation ($\bar{h}=1.0$).

(5) The only branch continues towards $L\rightarrow\infty$, A increases monotonously but not v (supercritical bifurcation, $\bar{h}=1.5$).

(6) Again, two branches exist, but only the low velocity branch continues towards $L\rightarrow\infty$. The ending branch shows a monotonic dependence of v on L, but the infinite branch is nonmonotonic (subcritical bifurcation, $\bar{h}=2.0$,$\bar{h}=2.5$ and $\bar{h}=2.86$). For $\bar{h}=2.5$, some profiles for different period are shown in Fig. 4.

(7) Nearly the same as (2), but here the branch with lower velocity corresponds to larger amplitude ($\bar{h}=3.5$).

(8) For very large $\bar{h}$ no solution exists beside the trivial one $h(x)=h_0$.

The flat film is linearly stable for the cases (1), (2), (7), and (8), but is linearly unstable for cases (3)–(6). Figures 2 and 3 show that for each family one branch converges to a line common for all families. Solutions along this line have a velocity and amplitude that are independent of the mean film thickness, i.e., independent of liquid volume, an observation that is explained later (Sec. IV B). The convergence to this line occurs at a lower period for larger mean film thickness than for small film thickness. For the linearly unstable mean film thicknesses, the branch that continues towards $L\rightarrow\infty$ is the converging branch whereas for the linearly stable mean film thicknesses (2) and (7) the converging branch is the high- and low-velocity branch, respectively. Also, the film profile converges to a common shape: a flat drop with an upper plateau of thickness h_u on a very thin (precursor) film called here lower plateau of thickness h_d. At the downstream front of the drop, the profile overshoots before relaxing further upstream to the upper plateau thickness, and hence, a capillary ridge forms. Only the length of the upper plateau depends on the mean film thickness. Before we embark on

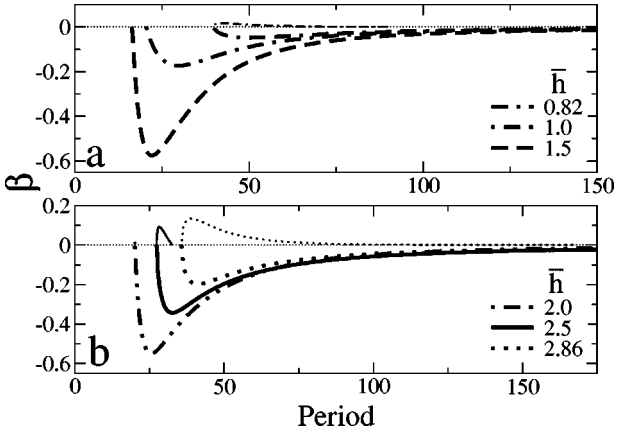

FIG. 5. Linear stability results for the periodic stationary solutions are given for different mean film thicknesses $\bar{h}$ as shown in the legends of (a) and (b). $G=0.1$, $\alpha=0.1$, and $a=0.1$. The thin and thick lines represent unstable and stable profiles, respectively.

the study of these ''universal'' flat drops in Sec. IV B, we will give an interpretation of the branches that do not converge to the common line.

As mentioned above in point (3), the critical wavelength λ_c where the flat film becomes linearly unstable can be seen as the locus of a bifurcation. Because the flat film is linearly stable for $\lambda<\lambda_c$, the subcritical branch in (3) and (6) starting at λ_c should consist of unstable solutions, whereas the supercritical branch starting in (4) and (5) at λ_c should consist of stable solutions. This is confirmed by calculating the growth rate for a small disturbance to the periodic solutions (see Appendix A) as shown in Fig. 5. The branches that terminate at λ_c are always linearly unstable, whereas the branches that continue towards an infinite period are always linearly stable taking one solution period as the unit of the stability analysis. Take note that there is a most stable solution on every (linearly stable) branch. Its period is slightly larger than the minimal period on the branch (Fig. 5) and is not correlated with λ_c. However, the linearly stable solutions are linearly unstable if one takes more than one solution period as the unit of the stability analysis. The latter corresponds to an instability with respect to coarse-graining modes as known from the case $\alpha=0$ [44], i.e., in the course of time the length scale of the pattern increases. However, the process slows down exponentially with increasing lengthscale and is not discussed further in this work. The coarse-graining instability was only checked for relatively small α. As discussed in Sec. V, at larger α there may be a crossover towards periodic solutions that are stable with respect to coarse graining. For the case $\alpha=0$, it was shown that the terminating branches represent nucleation solutions [44], i.e., these solutions represent critical finite disturbances for linearly stable but not absolutly stable (i.e., metastable) flat films. At constant shape, disturbances with smaller amplitude than the critical disturbance will relax in time towards the flat film solution, whereas an amplitude larger than critical leads to growth of the disturbance. The system will then reach the solution on the other, the stable branch. This interpretation is also valid in the case $\alpha\neq0$ as illustrated in

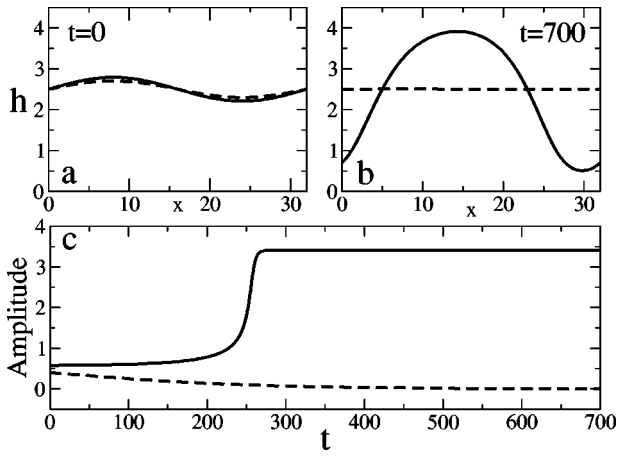

FIG. 6. Time evolution of a finite disturbance. At time $t=0$, a disturbance is given as $h_0+A_0\sin(2\pi/L)$ with $h_0=2.5$, $L=32$, $G=0.1$, $a=0.1$, and $\alpha=0.1$. The disturbance with $A_0=0.2$ shrinks (dashed line) whereas the one with $A_0=0.29$ (solid line) grows. Initial and final profiles are shown in (a) and (b), respectively. (c) gives the time evolution of the amplitude of the profile.

Fig. 6. The interpretation holds also for the nonuniversal branches that continue towards infinity in the cases (2) and (7).

B. Flat drops

Before we focus on the dependence of the properties of the flat drops on the system parameters, we want to identify what limits their existence as solutions. For large periods, the volume of liquid (mean film thickness) only influences the ratio χ between drop length l and the period of the solution L. The ratio is given by $\chi=(\bar{h}-h_d)/(h_u-h_d)$. Flat drops cannot exist for $\chi\to 0$ because there is not enough matter in the system to form a flat drop. For $\chi\to 1$, the downstream end of the drop approaches the upstream end of its predecessor and both ends start to interact: the profile then becomes a moving hole in a flat film or small nonlinear waves on an otherwise flat film. These solutions depend strongly on the mean film thickness and will be discussed in Sec. IV C.

At this point, only situations are studied where these restrictions do not apply. The solutions in this parameter range are flat drops whose plateau thicknesses depend on the parameters α, a, and G only. Choosing one of the two plateau thicknesses as h_0, the other plateau thickness is given as the second positive fixed point of Eq. (8), i.e., by Eq. (10). Only the ratio of the length of the upper to the lower plateau is influenced by the given liquid volume. The velocity of the flat drops is determined by the dynamic equilibrium between the overall forces of gravity acting on the liquid and viscous friction. The equilibrium does not depend on the liquid volume because both forces are proportional to the length of the flat drop.

Looking at Figs. 2 and 3, one observes that at period $L=500$, only the curves for relatively small mean film thicknesses have not yet reached the universal curve. To study the dependence of the plateau thicknesses h_u and h_d and velocity v on the inclination angle and interaction parameters, we fix

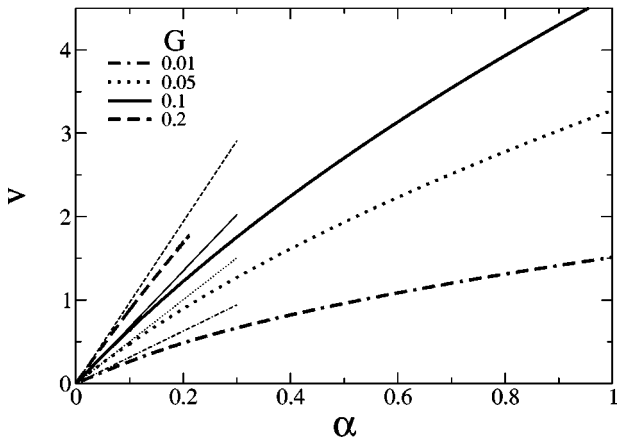

FIG. 7. The dependence of the velocity, v, on inclination angle α, for different G as given in the legend. The thick lines are universal curves that are independent of the mean film thickness, within the limits discussed in the main text. $a=0.1$ and $L=2000$. The thin lines represent the analytical results of Eq. (16).

the period at the value $L=2000$ where all curves $v(L)$ shown in Fig. 2 have reached the universal solution. First, a is fixed to study the dependence of v, h_u, and h_d on α, for different G. Recall that the scaled inclination angle α is not a small parameter contrary to the unscaled physical angle $\bar{\alpha}$.

The velocity increases monotonically with α (Fig. 7) and the flat drop becomes thinner by decreasing its upper-plateau thickness and increasing the lower-plateau or precursor film thickness (Fig. 8). In the limiting case α and $v\to 0$ and $G\ll 1$ the ratio v/α, i.e., the slope of the function $v(\alpha)$ at $\alpha=0$ may be estimated because the plateau thicknesses have to coincide with the values obtained for a drop on a noninclined plane ($\alpha=0$) [44]. These values depend only on the properties of the free energy $f(h)$ and are given for $G\ll 1$ by

$$h^d=\sqrt{G/2}+\frac{3}{8}G+O(G^{3/2}),$$

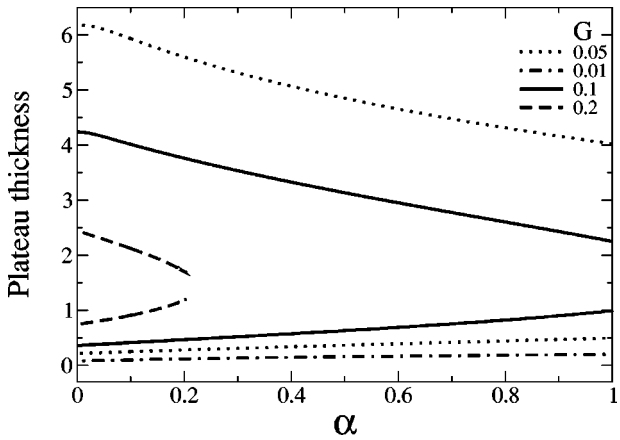

FIG. 8. Shown is the dependence of the two plateau thicknesses—the upper-plateau thickness h_u and the precursor film thickness h_d—on inclination angle α for different G as shown in the legend. Plotted is the universal part of the curves that is independent of the mean film thicknesses within the limits discussed in the text. $a=0.1$ and $L=2000$.

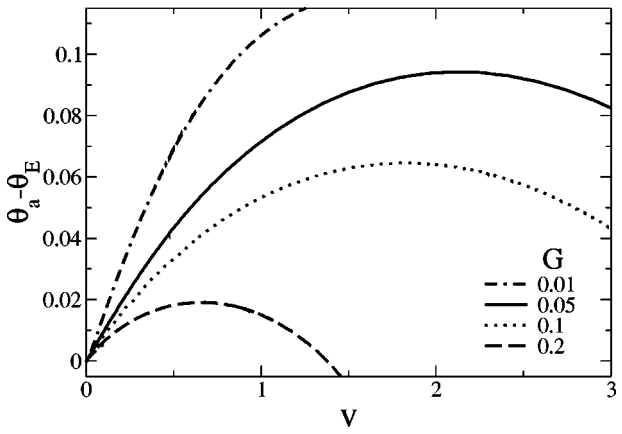

FIG. 9. The difference of the advancing dynamical contact angle θ_a and the equilibrium contact angle θ_E as a function of the drop velocity v for different G as shown in the legend. $a=0.1$ and $L=2000$.

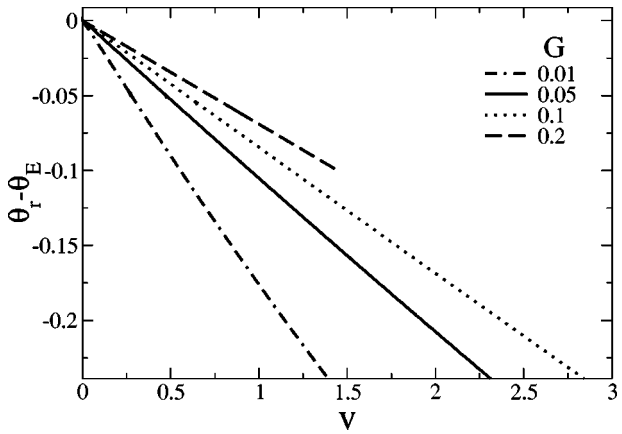

FIG. 10. The difference of the receding dynamical contact angle θ_r and the equilibrium contact angle θ_E in dependence of the drop velocity v for G as given in the legend. $a=0.1$ and $L=2000$.

and

$$h^u=\sqrt{2/G}-\frac{\sqrt{2}}{16}\sqrt{G}+\frac{21}{128}G+O(G^{3/2}). \tag{15}$$

Take note that $h^d\approx\sqrt{G/2}$ is the ''capillary length'' l_C of the problem. As in physical units $l_C=\sqrt{l\kappa/\rho g}$ one sees that $l\kappa$ plays the role of surface tension in a description of a drop without precursor film. $l\kappa$ may be identified as the difference in the surface energies between lower- and upper-plateau thicknesses, precursor film, and drop surface for $\alpha=0$ [44]. Inserting relations (15) in Eq. (10) results in

$$\left.\frac{v}{\alpha}\right|_{\alpha\to 0} \text{ tending to } \quad 2-3\sqrt{2G}\ln a+\left[\frac{3}{4}+3(\ln a)^2\right]G +O(G^{3/2}). \tag{16}$$

This gives already a good estimation for the slope of the curve $v(\alpha)$ at $\alpha=0$ as shown in Fig. 7. Note that for very small G, this slope approaches 2, i.e., in physical units $v=(2\kappa l/3\eta)\alpha$. The velocity scale is given by the ratio of the difference in surface energies and viscosity $\kappa l/\eta$.

Furthermore, we study the dependence of the dynamic contact angles on drop velocities. We define the contact angle as the absolute value of the slope of the profile at its inflection point. The drop has two dynamic contact angles, the advancing angle at its downstream front θ_a and the receeding angle upstream θ_r. The differences between these angles and the equilibrium or static contact angle θ_E, obtained for $\alpha=0$ are shown in Fig. 9 and Fig. 10, respectively. Let us first discuss Fig. 10. The receding angle is always smaller than θ_E and in the velocity range studied here, the absolute value of the difference between both angles increases linearly with increasing velocity. The increase becomes steeper with smaller G. However, Fig. 9 shows that the difference between the advancing angle and θ_E changes nonmonotonically with increasing velocity v. It increases for small v, but decreases for larger v. For relatively large velocities, θ_a may even become smaller than θ_E. The increasing part of the curve extends towards larger v with decreasing G. It was checked that the decrease is neither an effect of leaving the universal branch (interaction between drops) nor caused by further oscillations of the profile.

These further oscillations appear for even higher velocities: Increasing α enforces the overshooting at the front of the drop. The difference between upper plateau thickness and maximal height gets larger and secondary oscillations or ''wiggles'' evolve behind the capillary ridge and also in front of the drop (undershooting). As the range of the wiggles extends the back and the front of different drops start to interact. This is another way for the solutions to leave the universal branch. We conclude the analysis of the solution families with a study of the nonuniversal part of the branches.

C. Nonuniversal solutions

The solution families leave the universal curve of the flat drops mainly because one of the plateau thicknesses approaches the mean film thickness. Nonuniversal hole [drop] solutions arise when the upper- [lower]-plateau thickness comes close to $\bar{h}$. Further away from the universal curve both cases give rise to solitary waves of relatively small amplitude on an otherwise flat film. Let us follow, for instance, the upper curve for $G=0.1$ in Fig. 8. When increasing α for a mean film thickness $\bar{h}=3.0$, the upper-plateau thickness h_u approaches $\bar{h}$ at about $\alpha=0.5$, χ approaches 1 (Sec. IV B) and the solution family has to leave the universal flat-drop branch. This is shown in Fig. 11 where the velocity v is given as a function of α for various $\bar{h}$. This figure is the equivalent of Fig. 7 for the nonuniversal solutions. As expected, the point of departure from the universal branch depends strongly on the chosen $\bar{h}$. With decreasing $\bar{h}$, it shifts towards larger inclination angles. Complementary information for the same situation, that is the dependence of solution amplitude A on α, is given in Fig. 12.

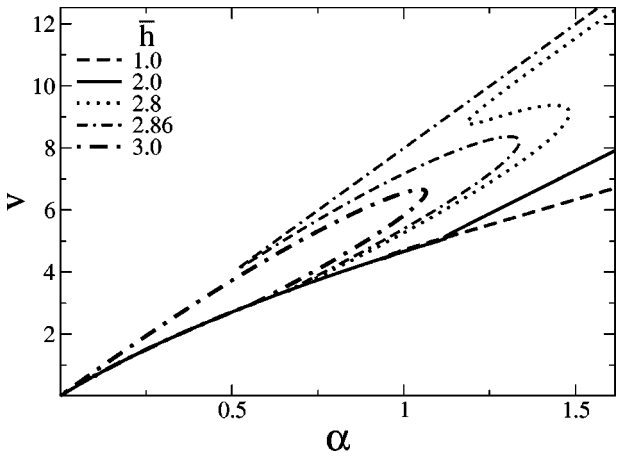

FIG. 11. The dependence of the velocity v on inclination angle α for different mean film thicknesses as given in the legend. $a=0.1$, $G=0.1$, and $L=2000$.

The nonuniversal part of the families consist of one, two, or three branches. Decreasing $\bar{h}$ we distinguish cases (a) to (c):

(a) Two branches exist, giving the $v(\alpha)$ curve a petallike shape. This implies the existence of two small α solutions ($\bar{h}=3.0$ in Fig. 7). The branch with higher velocity consists of solutions with smaller amplitude than the solutions of the other branch for identical α (Fig. 12). Solutions for $\bar{h}=3.0$ are shown in Fig. 13.

(b) Three branches exist, resulting in a broken-petal or *S*-like shape of the $v(\alpha)$ curve and a *Z*-like shape of the $A(\alpha)$ curve. The high-velocity branch of the $v(\alpha)$ dependence ($\bar{h}=2.86$ and 2.8 in Fig. 11) converges to the straight line $v=3\alpha G(\bar{h}-\ln a)^2$, i.e., the velocity of the small-amplitude solutions obtained in Sec. III B. Solution profiles for $\bar{h}=2.86$ are shown in Fig. 14.

(c) Only one branch exists, which also departs from the universal branch ($\bar{h}=1.0$ and 2.0 in Figs. 11 and 12).

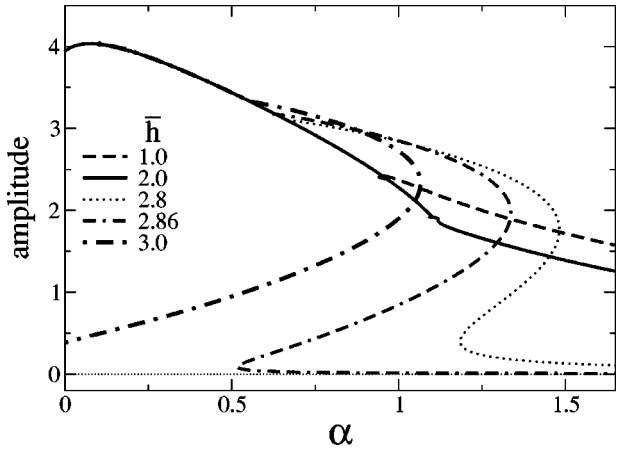

FIG. 12. The dependence of the amplitude on inclination angle α for $\bar{h}$ as given in the legend. $a=0.1$, $G=0.1$, and $L=2000$.

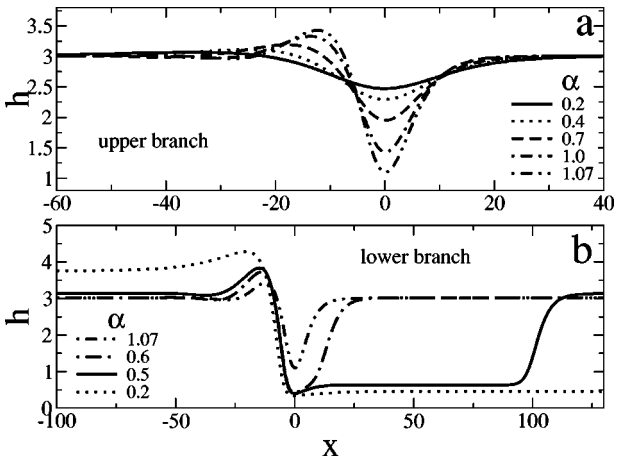

FIG. 13. Thickness profiles for different inclination angle α as given in the legends for $\bar{h}=3.0$, $G=0.1$, $a=0.1$, and $L=2000$. (a) and (b) show profils for the upper and lower branch of the curve with $\bar{h}=3.0$ in Fig. 11, respectively.

Our interpretation of the nonuniversal branches rests upon the results for the families obtained when changing the period (Sec. IV A). In the range of mean film thickness that corresponds roughly to metastable films for $\alpha=0$ [44], we encounter again the linearly unstable solutions, that were identified as periodic nucleation solutions. In case (a), the upper branch in the $v(\alpha)$ plot represents such linearly unstable solutions, whereas the lower branch is linearly stable. Taking the $\alpha\rightarrow 0$ limit, the solutions of the upper branch approach the respective solutions that represent periodic nucleation solution in the problem of film rupture on a horizontal plane [44]. Take note, that as in Sec. III we use one period of the respective solutions as the unit of the stability analysis. Thus, we determine whether a solution is linearly stable for a fixed period. It may be unstable to coarse graining as in [44].

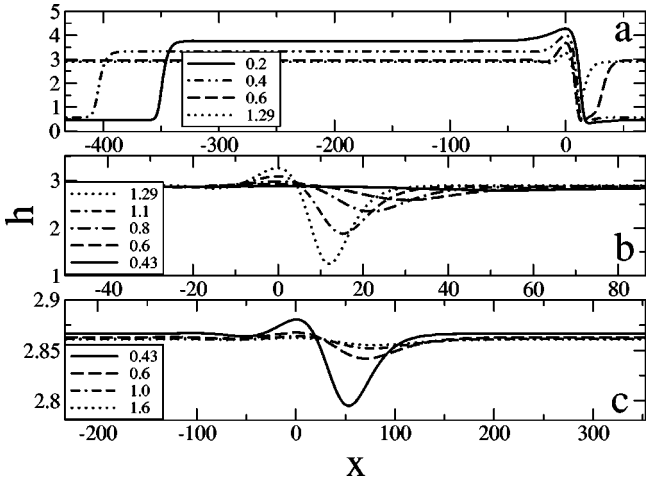

FIG. 14. Thickness profiles for different inclination angle α as given in the legends for $\bar{h}=2.86$, $G=0.1$, $a=0.1$, and $L=500$. (a), (b), and (c) show profils for the upper, medium, and lower branch of the curve with $\bar{h}=2.86$ in Fig. 11, respectively.

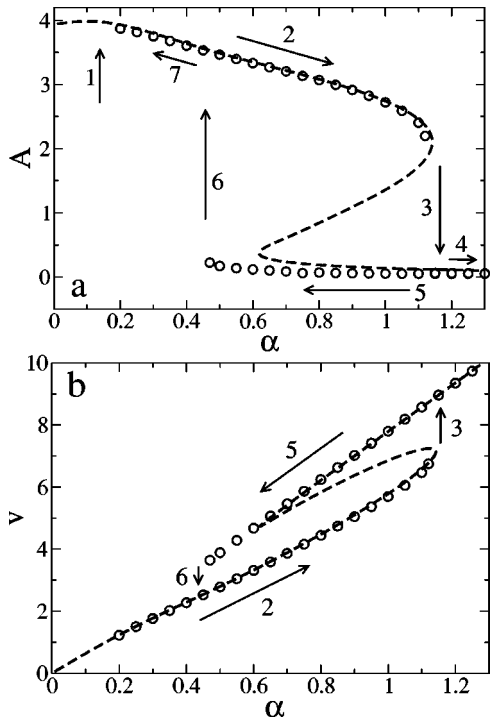

FIG. 15. Shown are (a) the amplitude A and (b) the velocity v as a function of the inclination angle α for the different steps of a time simulation for the hysteresis effect (open circles). The dashed lines show the families of stationary solutions as obtained by continuation. The arrows indicate the sequence in time that is further explained in the main text.

The middle branch in case (b) consists also of nucleation solutions. This is confirmed by the results of the linear stability analysis of the found periodic solutions, performed as outlined in the Appendix. For each branch, the real part of the largest eigenvalue, i.e., the growth rate of disturbances, determines the stability of the solutions. For (b), the middle branch has a positive growth rate as expected, whereas the two other branches are linearely stable because the largest nontrivial eigenvalue is negative. Besides the linearly stable large-amplitude branch already known from case (a), there also exist linearly stable small-amplitude solutions, identified as nonlinear surface waves. In the range of α where both stable branches exist they are separated by the unstable branch that acts as a nucleation solution: it has to be overcome from either side in order to jump to the other branch. This has two important effects: (I) An apparent stability of the flat film and (II) some hysteresis.

(I) Because the surface waves have very small amplitude [see Figs. 12 and 14(c)] they may be missed in an experiment focused on drop formation and the linearly unstable flat film may appear stable, because no evolution towards drop-like large-amplitude structures would take place.

(II) The existence of two linearly stable branches between inclination angles α_d and α_u gives rise to hysteresis: Changing α, one may jump from one linearly stable branch to the other. However, whereas the transition from the large- to the small-amplitude branch occurs at α_u, the transition from the small- to the large-amplitude branch occurs at α_d. The transition between the two branches may be called a *dynamical wetting transition with hysteresis*. Such a dynamical wetting transition is now reasonably well understood [40,47–49]: at the macro scale, it would occur when the contact angle vanishes at finite velocity. However, as far as we know, no hysteresis has been predicted and/or observed although it does not seem to be excluded at all from first principles.

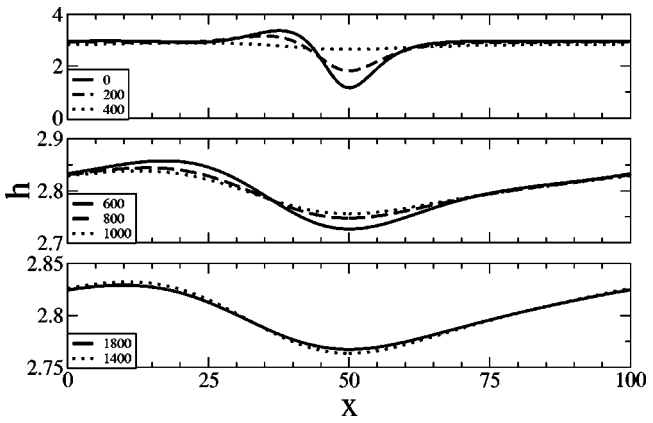

FIG. 16. Film thickness profiles are shown for different times as indicated in the legends for the jump from the large amplitude branch to the small amplitude branch symbolized by arrow (3) in Fig. 15. Take note of the large difference of the amplitude between the first curve and the last curve.

To show the hysteresis, we perform a numerical experiment as follows (see Fig. 15). A slightly disturbed, linearly unstable flat film flows on a plane with a relatively small inclination $\alpha_0 < \alpha_d$. Integrating Eq. (6) in time for the fixed period $L=100$ shows that the disturbance grows and the solution settles on the stable flat-drop branch as indicated by arrow (1) in [Fig. 15(a)]. Now, the inclination angle is increased slowly. After every (small) step, the flat drop reaches a dynamic equilibrium. Only some of them are shown as open circles in Fig. 15. The obtained series of profils follows the curve of the stationary solutions [arrow (2)]. Reaching the end of the linearely stable large-amplitude branch, the solution jumps to the small-amplitude solution branch when α passes α_u [arrow (3)]. Some snapshots of film thickness profiles during this jump are shown in Fig. 16.

When increasing [arrow (4)] or decreasing [arrow (5)] α the solution follows the branch of small amplitude nonlinear surface waves. Decreasing α, one has to wait until passing α_d to jump back to the flat drop branch indicated by arrow (6). Decreasing α further leaves the solution on the flat drop branch [Fig. 15(a), arrow (7)]. Take note that the return to the flat drop branch occurs at a $\alpha_d^{num} < \alpha_d$. This is probably due to the fact that the growth rate for the small-amplitude solutions approaches zero where the two solutions meet implying a critical slowing down of the dynamics of relaxation towards the stationary solution for the next value of α. Accordingly, the jump may only be seen when the system is far enough away from the end point of the branches. The locus of this jump depends slightly on the spacial grid resolution employed in the time integration.

V. CONCLUSION

We have analyzed the evolution of a thin liquid film flowing down an inclined plane taking into account the interaction with the substrate. The latter is modeled by a disjoining pressure arising in a recent theory derived from coupled van der Waals equations and thin-film hydrodynamics [42]. We have studied the flat film solutions and their linear stability. As a result we found, that although the thickness of the flat film solutions depends on velocity and inclination angle, their linear stability is independent of these dynamical aspects. The linear stability of the flat film is determined only by the first derivative of the disjoining pressure as for film rupture on a horizontal substrate [44].

Using small-amplitude stationary solutions as a starting point, continuation techniques allowed to calculate families of finite-amplitude stationary solutions. Depending on mean film thickness, different types of solution families were found and classified. Linear stability analysis showed the existence of linearly stable solutions and linearly unstable nucleation solutions. Although for small inclination angles there are solution families that correspond to the family types found on the horizontal plane [44], there are significant differences. First the solutions are asymmetric and slide down the inclined plane. Secondly, the dependence of the velocity on solution period also varies strongly with mean film thickness, a behavior that clearly has no counterpart in the noninclined case. Beside the families that have a counterpart in the case $\alpha=0$, there exist stationary nonlinear surface waves that are specific for $\alpha\neq 0$. They do only exist if both molecular interaction and viscous flow driven by gravitation are present and depend strongly on the ratio of mean film thickness and length scale of the diffuse interface.

The study of the solutions as a function of the period revealed the existence of universal flat drop solutions. Their velocity and plateau thicknesses do not depend on period and mean film thickness. They have the form of flat liquid sheets of different length and end downstream with a capillary ridge. The dependence of the properties of the flat drops on inclination angle and interaction parameters was determined. With increasing inclination angle, the upper- [lower-]-plateau thickness decreases [increases], the velocity increases, and the receeding dynamic contact angle decreases. The advancing dynamic contact angle shows a nonmonotonic behavior as a function of the velocity, it increases first then decreases even below its static equilibrium value. The effect is more pronounced for larger G.

The universal regime breaks down if one of the plateau thicknesses approaches the mean film thickness. The study of the nonuniversal families has revealed an hysteresis effect, when jumps between a small- and a large-amplitude solution occur that both exist for a certain range of inclination angles for some mean film thicknesses. The existence of the branch of stable small-amplitude solutions may in an experiment lead to the impression of stable flat film flow in the linearly unstable mean thickness range, because no large amplitude solutions can be seen without overcoming a nucleation solution. The occurring surface wave may go unnoticed because of its very small amplitude.

We have investigated the main effects occuring in a system where viscous stress and molecular interactions are dominant. The overall picture may be well understood and visualized for small but not very small G, a parameter describing the ratio of gravitation to molecular interactions. In real physical situations, this ratio is normally very small, implying that the results shown here do only qualitatively resemble drop profiles or velocities occuring in nature. Numerical calculations showed that all qualitative features are also found for very small G. In order not to confuse the reader we normally did not change the interaction parameter a in this paper. It has an influence on the time scale of the dynamics of the system and also shifts borders in parameter space between the occurrence of different family types. However, the study of these details is not the scope of this paper.

Most works [27,35,50] on liquid sheets or ridges flowing down an inclined plane analyze separately the three regions; (1) upstream end, (2) central part, and (3) downstream end of the ridge. Similarity solutions in the regions (1), (2), and (3) are determined and matched together. The power dependence on time in these models is due to the fact that the situations studied are a superposition of spreading and sliding going on forever although we look at sliding droplets of constant shape in a moving frame as observed by Podgorski [40]. Because of the continuing time dependence the stability analysis for the leading edge (1) depends nontrivially on time through changing matching conditions, i.e., the changing ratio of upstream film thickness and precursor film thickness or slip length as happens in [31,50]. In slip models, the dynamic contact angle is explicitly fixed at the contact line [31,36] or varies in a prescribed way with velocity [35]. In the precursor film models, however, the contact angle is zero without motion although with motion a dynamic contact angle depends on the velocity of the advancing front.

Here, we do not study the superposition of spreading and sliding, but the stationary movement of drops, i.e., we study drops that do not change their shape and move with a constant velocity. When the inclination angle vanishes, the shape of our droplets converges to the equilibrium shape on a horizontal plane. All the ad hoc parameters in the above approach (static and dynamic contact angle, drop velocity, drop and precursor film thickness) are deduced within our theory from the two parameters describing wetting properties and ratio of molecular interaction to gravitation, respectively. For small liquid volume in an individual drop also the volume influences the drop properties.

An analysis similar to the one performed here could also be used to analyze liquid films on an inclined plane under the influence of other disjoining pressures, as for instance used in Refs. [1,5]. We think that the main qualitative results will be very similar for other disjoining pressures also combining destabilizing short-range and stabilizing long-range interactions. However, as was shown for liquid films on a horizontal plane [44,51], results may differ in important details, due to the different behavior of the various disjoining pressures at vanishing film thickness. Different behavior is to be expected for other types of disjoining pressure, as for instance the

combination of stabilizing short-range and destabilizing long-range interactions.

The rupture of a thin-liquid film on a horizontal substrate is closely related to the decomposition of a binary mixture as described by the Cahn-Hilliard Eq. [9,44,52]. Thus, the problem treated here has a close relation to convective Cahn-Hilliard models [53]. Close to the critical point ($G_c = 1/4, h_c = \ln 4$) (Sec. III B) the disjoining pressure may be expressed as a cubic [44] and Eq. (6) takes the form

$$\partial_t \epsilon = -\partial_x \left\{ (h_c - \ln a + \epsilon)^3 \left[\partial_x \left(\partial_{xx}\epsilon - \frac{f_4}{6}\epsilon^3 - g\epsilon \right) + \alpha g \right] \right\}, \tag{17}$$

where we introduced the small deviations ϵ and g by $h(x) = h_c + \epsilon(x)$ and $G = G_c + g$; and f_4 stands for $\partial_{hhhh} f|_{h_c}$. Assuming $\epsilon \ll 1$, $g = O(\epsilon)$, $f_4 = O(\epsilon^{-1})$, $x = O(\epsilon^{-1/2})$, $\alpha = O(\epsilon^{-1/2})$, and $t = O(\epsilon^{-2})$, Eq. (17) reduces to

$$\partial_t \epsilon = -\partial_{xx}\left[\partial_{xx}\epsilon - \frac{f_4}{6}\epsilon^3 - g\epsilon \right] + \frac{6\alpha g}{h_c^2}\epsilon\partial_x \epsilon. \tag{18}$$

The usual Cahn-Hilliard equation is Eq. (18) without the last term. Equation (18) may further be transformed by another scaling of t, x, and h into the convective Cahn-Hilliard equation studied in [53], which itself is related to the Kuramoto-Sivashinsky equation used to describe formation of small-amplitude structures on falling liquid films [1]. So, it is expected that an analog of the described dynamical wetting transition with hysteresis may be found in the convective Cahn-Hilliard model and that further studies of Eqs. (18) and (6) will reveal periodic drop structures stable against coarse graining.

ACKNOWLEDGMENTS

This research was supported by the European Union under ICOPAC Grant No. HPRN-CT-2000-00136, by the German Academic Exchange Board (DAAD) under Grant No. D/98/14745, by the Deutsche Forschungsgemeinschaft under Grant No. TH781/1, and by the Spanish Ministry of Education and Culture under Grant No. PB 96-599. We would like to thank U. Bahr, G. Diener, and E. Knobloch for helpful discussions.

APPENDIX A: NUMERICAL METHODS

Finite-amplitude periodic solutions of Eq. (8) are calculated by continuation [46]. The small-amplitude solutions obtained in Sec. IV A are used as starting solutions and are continued through the parameter space. One may vary the period of the solutions L, their mean film thickness $\overline{h}$, the inclination angle of the plane α, or the interaction parameters G and a. Studying solutions with large periods, we get good approximations for localized solutions, such as sliding holes and drops or moving fronts or kinks (hydraulic jumps).

We fix, for example, $\overline{h}$, G, and a, use periodic boundary conditions for h, $\partial_x h$, and $\partial_{xx} h$ and look for solutions with different period. To break the translational symmetry of the solutions and therefore to eliminate the trivial dimension of the solution space we have to pin the solution demanding for example $\partial_x h(0) = 0$. The resulting four boundary conditions and the integral condition of fixed mean film thickness allow us to determine the two missing parameters v and C_0 for every period, L.

The stationary solutions are further studied by determining their linear stability. This is done by adding a small time-dependent disturbance $\epsilon h_1(x)\exp \beta t$ to the stationary solution $h_0(x)$. Linearizing Eq. (6) transformed into the comoving frame in ϵ results in an eigenvalue problem for the growth rate, β, and disturbance, $h_1(x)$,

$$\begin{aligned}\beta h_1 = &\{[3q^2(h_{0x}f_{hh} - h_{0xxx})]_x + (q^3 h_{0x} f_{hhh})_x\} h_1 \\ &+ [2q^3 h_{0x} f_{hhh} + 3q^2(2h_{0x}f_{hh} - h_{0xxx})] h_{1x} \\ &+ q^3 f_{hh} h_{1xx} - 3q^2 h_{0x} h_{1xxx} - q^3 h_{1xxxx} \\ &- (3\alpha G q^2 h_1)_x + v h_{1x},\end{aligned} \tag{A1}$$

where $q = h_0(x) - \ln a$ and all derivatives of f are functions of the periodic solution $h_0(x)$. For a disturbed flat film Eq. (A1) reduces to Eq. (11).

To solve numerically Eq. (A1), we discretize it by expressing the derivatives of $h_1[i]$ at a point i as a linear combination of $h_1[n]$ where $i-2 \leqslant n \leqslant i+2$. Using periodic boundary conditions, this yields the algebraic eigenvalue problem:

$$\beta h_1 + \mathbf{S}(h_0, h_{0x}, h_{0xx}, h_{0xxx}, h_{0xxxx}, f_h, f_{hh}, f_{hhh}) h_1 = 0, \tag{A2}$$

where $\mathbf{S}$ is a linear operator determined by the periodic solution, h_0. We search for the largest eigenvalues (i.e., growth rates) β and the corresponding eigenvectors h_1. In the problem studied, the largest eigenvalue is always real. In this stability analysis, one cannot use solutions with large periods such as $L = 2000$ because of the necessary equidistant discretization in space. Therefore, the stability calculation in Sec. IV C is done for the relatively small period $L = 100$. This is feasible in a range of film thicknesses and periods where the characteristics of the branches, especially, begin and end point of the middle branch for the broken-petal curves depend only slightly on L.

Numerical integration of the time-dependent Eq. (6) is used to confirm the interpretation of the stationary solutions. We used a semi-implicit pseudospectral code and integrated Eq. (6) on a grid of 1024 (for $L = 100$) or 512 (for $L = 32$) mesh points. To avoid numerical instabilities for large amplitudes, we had to choose a small timestep of $dt = 1.e-4$. The code was implemented on a Alpha Workstation XP1000. The simulation took a couple of hours of CPU time to reach a stationary state, moving with a constant velocity as shown, for instance, in Fig. 6.

For the hysteresis part (Sec. IV C), we started with the small inclination angle $\alpha = 0.2$ and increased it adiabatically using normally steps of $\Delta\alpha = 0.05$, and steps of $\Delta\alpha = 0.01$ near the transitions points α_u and α_d. After reaching $\alpha = 1.4$, we decreased α again and returned stepwise as before until reaching the initial value.

[1] A. Oron, S. H. Davis, and S. G. Bankoff, Rev. Mod. Phys. **69**, 931 (1997).
[2] P. de Gennes, Rev. Mod. Phys. **57**, 827 (1985).
[3] B. V. Derjaguin, Zh. Fiz. Khim. **14**, 137 (1940).
[4] B. V. Derjaguin, N. V. Churaev, and V. M. Muller, *Surface Forces* (Consultants Bureau, New York, 1987).
[5] G. F. Teletzke, H. T. Davis, and L. E. Scriven, Rev. Phys. Appl. **23**, 989 (1988).
[6] R. J. Hunter, *Foundation of Colloid Science*, Vol. 1 (Clarendon Press, Oxford, 1992).
[7] J. N. Israelachvili, *Intermolecular and Surface Forces* (Academic Press, London, 1992).
[8] V. M. Starov, Adv. Colloid Interface Sci. **39**, 147 (1992).
[9] V. S. Mitlin, J. Colloid Interface Sci. **156**, 491 (1993).
[10] G. Reiter, Phys. Rev. Lett. **68**, 75 (1992).
[11] E. Ruckenstein and R. Jain, J. Chem. Soc., Faraday Trans 2 **70**, 132 (1974).
[12] A. Sharma and A. T. Jameel, J. Colloid Interface Sci. **161**, 190 (1993).
[13] A. Sharma and R. Khanna, Phys. Rev. Lett. **81**, 3463 (1998).
[14] A. Oron, Phys. Rev. Lett. **85**, 2108 (2000).
[15] A. M. Cazabat, Contemp. Phys. **28**, 347 (1987).
[16] L. Hocking, Phys. Fluids **6**, 3224 (1994).
[17] V. E. B. Dussan, Annu. Rev. Fluid Mech. **11**, 371 (1979).
[18] P. Kapitza and S. Kapitza, Zh. Exp. Teor. Fiz. **19**, 105 (1949); also in *Collected Papers of P. L. Kapitza*, edited by D. ter Haar (Pergamon, Oxford), pp. 690–709.
[19] J. Liu and J. Gollub, Phys. Fluids **6(5)**, 1702 (1994).
[20] T. B. Benjamin, J. Fluid Mech. **2**, 554 (1957).
[21] C. Yih, Phys. Fluids **6**, 321 (1963).
[22] D. Benney, J. Math. Phys. **45**, 150 (1966).
[23] W. Y. Shkadov, Izv. Akad. Nauk SSSR, Mekh. Zhidk. Gaza **1**, 43 (1967).
[24] B. Gjevik, Phys. Fluids **13**, 1918 (1970).
[25] S. Lin, J. Fluid Mech. **63**, 417 (1974).
[26] A. Pumir, P. Manneville, and Y. Pomeau, J. Fluid Mech. **135**, 27 (1983).
[27] H. E. Huppert, Nature (London) **300**, 427 (1982).
[28] N. Silvi and V. E. B. Dussan, Phys. Fluids **28**, 5 (1985).
[29] L. Hocking, J. Fluid Mech. **79**, 209 (1977).
[30] H. Greenspan, J. Fluid Mech. **84**, 125 (1978).
[31] N. Spaid and G. Homsy, Phys. Fluids **8**, 460 (1996).
[32] L. W. Schwarz, Phys. Fluids **1**, (1989).
[33] L. Hocking and M. Miksis, J. Fluid Mech. **247**, 157 (1993).
[34] D. E. Kataoka and S. M. Troian, J. Colloid Interface Sci. **192**, 350 (1997).
[35] L. Hocking, J. Fluid Mech. **211**, 373 (1990).
[36] D. Moyle, M.-S. Chen, and G. Homsy, Int. J. Multiphase Flow **25**, 1243 (1999).
[37] Y. D. Shikhmurzaev, J. Fluid Mech. **334**, 211 (1997).
[38] L. Mahadevan and Y. Pomeau, Phys. Fluids **11**, 2449 (1999).
[39] D. Richard and D. Quere, Europhys. Lett. **48**, 286 (1999).
[40] T. Podgorski, Ph.D. thesis, University of Paris, 2000.
[41] D. M. Anderson, G. B. McFadden, and A. A. Wheeler, Annu. Rev. Fluid Mech. **30**, 139 (1998).
[42] L. M. Pismen and Y. Pomeau, Phys. Rev. E **62**, 2480 (2000).
[43] However, the notation ''interaction'' is, after all, rather vague: The exponential interaction between substrate and liquid-gas interface is derived from thick interface theory, but it is not obviously present as a ''molecular'' interaction in the local van der Waals equation. This difficulty, namely, the difference between molecular interaction and effective interaction between mesoscale objects such as interfaces and surfaces, is often overlooked in works on the topic.
[44] U. Thiele, M. G. Velarde, K. Neuffer, and Y. Pomeau, Phys. Rev. E **64**, 031602 (2001).
[45] L. Nguyen and V. Balakotaiah, Phys. Fluids **12**, 2236 (2000).
[46] E. Doedel, A. Champneys, T. Fairfrieve, Y. Kuznetsov, B. Sandstede, and X. Wang, *AUTO97: Continuation and Bifurcation Software for Ordinary Differential Equations* (Concordia University, Montreal, 1997).
[47] T. Blake and K. Ruschak, Nature (London) **282**, 489 (1979).
[48] Y. Pomeau, C. R. Acad. Sci., Ser. IIb: Mec., Phys., Chim., Astron. **328**, 1 (2000).
[49] B. Ben Amar, L. Cummings, and Y. Pomeau, C. R. Acad. Sci., Ser. IIb: Mec., Phys., Chim., Astron. (to be published).
[50] S. Troian, E. Herbolzheimer, S. Safran, and J. Joanny, Europhys. Lett. **10**, 25 (1989).
[51] U. Thiele, M. G. Velarde, and K. Neuffer, Phys. Rev. Lett. **87**, 016104 (2001).
[52] J. W. Cahn and J. W. Hillard, J. Chem. Phys. **28**, 258 (1958).
[53] A. Golovin, A. Nepomnyashchy, S. Davis, and M. Zaks, Phys. Rev. Lett. **86**, 1550 (2001).